

Shock Acceleration in Hot Spots

M. H. Pope, Lewis Ball and D. B. Melrose

Research Centre for Theoretical Astrophysics,
University of Sydney, NSW 2006, Australia
ball@physics.usyd.edu.au

Received 1994 September 6, accepted 1995 May 31

Abstract: A simple model is presented for electron acceleration in extragalactic radio sources with two hot spots. The effect of diffusive shock acceleration by multiple shocks is calculated numerically, with adiabatic and synchrotron losses included. It is found for the sources 3C 20 and 3C 268.4 that a consistent set of model parameters exists which reproduce the observations. The model fails to reproduce the observations for the source 3C 196.

Keywords: active galactic nuclei — particle acceleration — shock waves

1 Introduction

Hot spots are a characteristic feature of extragalactic radio sources. In a subset of such sources there are two hot spots, a primary and a secondary, and it has been suggested that there is a causal link between them (e.g. Cox, Gull & Scheuer 1991, hereafter CGS). Our objective in this paper is to answer the following question: Can the spectral indices of the hot spots, in sources which have both a primary and a secondary, be reproduced by diffusive shock acceleration (hereafter DSA)? More specifically, is reacceleration at the secondary hot spot of electrons initially accelerated at the primary necessary to account for the spectral differences between the secondary and the primary? Thus we seek to identify a consistent set of parameters which allows us to model the secondary in terms of reacceleration of electrons from the primary.

The primary hot spot is the site where the jet first impacts upon the external medium. Our model of the primary hot spot consists of (i) a shock where DSA occurs, with (ii) a downstream region of constant magnetic field. The secondary spot is modelled in the same way. In between the two hot spots (downstream of the constant magnetic field region associated with the primary hot spot) there is assumed to be a region where expansion losses occur. The expansion is that which occurs as the downstream flow expands from the size of the primary to that of the secondary hot spot. The sizes of the constant magnetic field regions are estimated from the observed sizes of the hot spots. Synchrotron emission is assumed to occur in the constant magnetic field regions. Further details of the model are discussed in Section 3. The results are presented and discussed in Section 4.

2 Previous Work

2.1 Observations

The standard model for classical, edge-brightened, double radio sources (Fanaroff & Riley class II, or FR II; Fanaroff & Riley 1974) is that of radio lobes fed by a narrow jet from the radio core. The observed hot spots, which are characterised by their high surface brightness and location near the outermost boundaries of the radio lobes (Bicknell 1985), are interpreted as the working surfaces of supersonic jets (Blandford & Rees 1974). However, many extragalactic radio sources (at least one-sixth of all 3CR sources with hot spots; Valtaoja 1984) do not fit the standard model. These sources exhibit multiple structures (Laing 1988) with, in most cases, a primary and a secondary hot spot. The primary hot spots (a) are compact ($<0.5 - 2 h^{-1}$ kpc, where $h = H_0/100 \text{ km s}^{-1} \text{ Mpc}^{-1}$); (b) contribute little to the flux density of the source; (c) are located at the sides of the lobes, set slightly back from the leading edges; (d) where resolved, are elongated towards the secondary, are joined to the secondary by a bridge of emission, and the magnetic field is orientated along a line joining the two; and (e) have high internal energy densities. The secondary structures take the form of either a discrete region, or a curved emitting region expanding away from the primary, known as a flaring hot spot (Laing 1988). Relative to the primary, the discrete secondary (a) is more diffuse; (b) has a steeper radio spectrum; (c) has a weaker magnetic field; (d) is not as luminous; and (e) has a greater total internal energy.

Valtaoja (1984) found that both the size and the internal energy of the secondary are correlated with the distance between the hot spots. In particular,

$$S_2 \propto D, \quad (1)$$

and

$$E_2/(E_1)^{\frac{1}{2}} \propto D^2, \quad (2)$$

where S_2 is the size of the secondary, D the distance between the hot spots, and E is the total internal energy. The subscripts 1 and 2 are used to denote the primary and secondary hot spots respectively. The relations (1) and (2), together with the alignment of the primary's magnetic field and its elongation towards the secondary, suggest that the secondary hot spot is fed by the primary. However, Valtaoja (1984) also found that there is no preferred orientation for the secondary, that is, it is equally likely to be closer to or further from the core than the primary. This poses difficulties for models which attempt to explain how the primary feeds the secondary.

2.2 Formation of Multiple Hot Spots

Four models exist in the literature which take into account the evidence for energy supply between the two hot spots, namely those of Williams & Gull (1984, hereafter WG; see also Williams 1991), Lonsdale & Barthel (1986, hereafter LB), Wilson (1988) and CGS.

2.2.1 The cloud model

The LB model invokes a massive ($10^8 M_{\odot}$), dense ($\geq 10^{-3} \text{ cm}^{-3}$) cloud with which the jet collides, forming the primary hot spot. The jet penetrates the cloud, becomes subsonic, and then inflates the cloud. Asymmetry results in a weak spot in the wall of the cloud, forming a de Laval nozzle so that the flow of escaping material through it becomes supersonic. This flow then feeds the secondary. This model is able to account for the apparently random orientation of the secondary with respect to the primary. However, a major uncertainty, as noted by LB, is whether such clouds exist.

2.2.2 The 'splatter' model

A 'splatter' model was proposed by WG. In this model, the jet precesses from its current site of impact to a new site. The jet then interacts obliquely with the jet cocoon wall, and forms an oblique shock wave. The jet passes through this shock without being disrupted, and is deflected by the shock to form a 'splatter spot' on the opposite side of the radio lobe. This splatter spot is further from the radio core than the primary hot spot. As this model evolves, the primary advances more rapidly than the secondary and may eventually overtake it. At some stage the secondary ceases to be fed by the primary and subsequently fades due to expansion and synchrotron losses.

A criticism of this model is that it is at odds with the observation that there is no tendency for

the primary to be closer to the core than the secondary.

2.2.3 The 'wall jet' model

The 'wall jet' model suggested by Wilson (1988) is based on the splatter model of WG, but with one important difference that is motivated by results from laboratory experiments on supersonic gas jets (Lamont & Hunt 1980). In these experiments, a supersonic gas jet impinges on a flat plate inclined at various angles of incidence. The jet passes through a shock above the plate and then, after passing through the high-pressure post-shock region, is accelerated through a transonic rarefaction wave and out into a thin, supersonically moving layer. This layer of gas is known as a wall jet. The flow is, in general, not in pressure equilibrium with the surrounding gas, resulting in a series of shocks and rarefactions. When the plate is inclined at an oblique angle, there is a preferred direction for the wall jet. Wilson (1988) suggested that the flow from a primary hot spot would not bounce off, as in the WG model, but would flow around the cavity wall. The wall jet only exists for a finite time until the jet has penetrated the cavity wall. Such wall jets could account for flaring hot spots.

2.2.4 A modified 'splatter model'

As mentioned above (Section 2.2.2), the WG model evolves in time until the primary hot spot no longer feeds the secondary. CGS performed three-dimensional simulations of a constantly precessing jet. They found that significant splatter spots do not have time to form in a rapidly precessing jet. However, a double hot spot structure is still observed—the primary is the current site of impact of the jet and the secondary is an aging primary. When the jet first starts to precess, the situation is still roughly axisymmetric, and the jet continues to feed the primary. As the jet precesses further, it strikes the cocoon wall upstream of the primary, forming an oblique shock, and the flow is diverted along the cocoon wall, still depositing most of its energy in the primary. As the jet impinges on the cocoon wall, a backflow forms and cuts off the flow to the secondary. However, there is still material flowing from the primary to the secondary at the time this cutoff occurs (called a disconnection event by CGS), and so the secondary is still fed for some time afterwards.

In the case of a more slowly precessing jet, there is time for a splatter spot to form, analogous to the WG model, where the jet precesses to its new position and then does not move.

CGS discussed the likely difference in appearance between the two types of secondaries. They claimed that the double hot spots in both lobes of Cygnus A are due to slowly aging old primaries, and that

the eastern lobe of 3C 20 (Laing 1981) is likely to be a splatter spot. Another likely candidate for a splatter spot is the northern lobe of 3C 196 (Lonsdale & Morison 1983), and the southern lobe of 3C 268.4 (Lonsdale & Barthel 1986).

3 The Model

The theory of DSA (see Kirk 1994 for a recent review) has been successfully applied to 'classical doubles' (Meisenheimer et al. 1989, hereafter M89). Two models which have included multiple accelerations in the lobes of radio galaxies are those of Gopal-Krishna & Wiita (1990) and Anastasiadis & Vlahos (1993). Gopal-Krishna & Wiita considered adiabatic compression by several shocks, whereas Anastasiadis & Vlahos considered shock drift acceleration. Both considered losses due to synchrotron radiation, but neglected expansion losses. In our model we assume DSA and include both synchrotron and expansion losses.

Our model is based on that of CGS. The jet encounters an oblique shock, the primary hot spot, where electrons are accelerated by DSA. We assume that the standard test-particle treatment is valid. There are two assumptions we must then justify. Firstly, relativistic oblique shocks may become superluminal, making diffusive acceleration unviable if particles are tied to the magnetic field lines. This is avoided by assuming that efficient cross-field diffusion occurs. The blast waves of young supernova remnants (of age <15 yr) are likely to be superluminal and are thought to be sources of energetic particles due to diffusive acceleration. It has been shown (Achterberg & Ball 1994) that resonant scattering by MHD waves, and magnetic field line wandering, may result in efficient cross-field diffusion and thus allow diffusive acceleration at superluminal oblique shocks. We assume that one or both of these mechanisms is operating in the primary hot spot. Secondly, efficient acceleration implies that the accelerated particles form a precursor to the shock, thus changing the total compression ratio that incoming particles experience. This modification is consistent with our treatment of the accelerated electrons as test particles, because we include the shock strength r as a model parameter obtained by fitting the observations, rather than making an *a priori* choice of the shock strength. After being accelerated by the shock, the electrons travel downstream through a region of constant magnetic field. We assume that this region is of length l_{\min} , the length of the minor axis of the primary. The electrons undergo synchrotron losses in this region, and the radio spectrum of the primary hot spot is taken to be the integrated emission from this constant-field region (M89; Kirk 1994). The electrons then continue on to the secondary, undergoing only expansion losses. At the secondary

hot spot the electrons are accelerated again, and subsequently lose energy again via synchrotron losses in a second region of constant magnetic field.

3.1 The Injection Spectrum

The injected electrons are assumed to be relativistic, being supplied by the jet. For the synchrotron spectra for the jets of the objects of interest, we use the result of Bridle & Perley (1984): $\sim 40\%$ of jets have $0.6 \leq \alpha_j \leq 0.7$, and $\geq 90\%$ have $0.5 \leq \alpha_j \leq 0.9$ (where $S_{j,\nu} \propto \nu^{-\alpha_j}$), where the subscript j denotes the jet values. More specifically, Laing, Riley & Longair (1983) found that $\langle \alpha_j \rangle = 0.78 \pm 0.015$ for the FR II sources in the 3CR catalogue. The spectral index of the electron momentum distribution is related to that of the synchrotron spectral distribution b_j by $b_j = 2\alpha_j + 3$, so the momentum spectral index is in the range $4 \leq b_j \leq 4.8$. The injection spectrum is written as

$$f_{\text{inj}}(p) = \frac{(b_j - 3)n_e}{4\pi p_1^3} \left(\frac{p}{p_1}\right)^{-b_j}, \quad (3)$$

where n_e is the electron number density of the jet, and p_1 is the lower cutoff momentum. The range of the distribution is taken to be $1.2 < p/(m_e c) < 1.2 \times 10^5$, where the lower cutoff is chosen so that the characteristic frequency at which electrons at this energy radiate is below 10 MHz for the magnetic field strengths used in the model.

3.2 The Acceleration Process

Diffusive acceleration of an upstream momentum distribution $f_-(p)$ leads to a downstream distribution $f_+(p)$ which may be written as (Kirk 1994)

$$f_+(p) = bp^{-b} \int_0^p dp' p'^{(b-1)} f_-(p'),$$

$$b = \frac{3r}{r-1}, \quad r = \frac{u_-}{u_+}, \quad (4)$$

where u_- is the upstream flow speed and u_+ is the downstream flow speed, both measured in the shock rest frame. Particles diffuse back and forth across the shock with diffusion coefficient κ . The strength of the shock in the primary hot spot (r_1) is one of our model parameters. The shock strength decreases with increasing obliquity of the shock (Williams 1991). Here we simply choose a shock strength and assume that the obliquity is small enough not to disrupt the flow, i.e. that the post-shock flow is still supersonic.

Standard DSA theory includes a δ -function contribution to the pre-acceleration spectrum, corresponding to the fraction of thermal particles injected. Such particles could either come from entrainment, or be particles which have cooled between the shocks. We do not include such a contribution in our treatment.

The maximum momentum to which the shock can accelerate particles is given by

$$\frac{p}{m_e c} = 1.2 \times 10^8 \frac{u_j}{B^{\frac{1}{2}}} \left[\frac{r-1}{r(r+1)} \right]^{\frac{1}{2}} \quad (5)$$

(Webb, Drury & Biermann 1984), where the jet speed u_j is in units of 10^3 km s^{-1} and B is in nT.

3.3 The Synchrotron Spectra

3.3.1 Synchrotron losses

To interpret observations of hot spots, it is important to take into account the fact that a telescope integrates over a region of finite size. Observations of a hot spot therefore include the emission from the shock and from some region of the downstream plasma. We assume that the magnetic field B is approximately constant in this downstream region (M89). In the Mach disks considered by M89 this region extends from the shock to the stagnation point of the post-shock flow. In an oblique shock, there is no stagnation point of the post-shock flow. The flow is bent by the oblique shock to follow the cocoon wall. This is our justification in assuming the existence of a region downstream of the shock, where the magnetic field is constant. In a Mach disk, the direction of the velocity vectors changes dramatically at the stagnation point, and the flow is diverted around into a backflow. In the case of an oblique shock, the flow is diverted not at a stagnation point, but by a rarefaction wave which increases the velocity of the jet. Following M89, we assume that the constant magnetic field region is of length l_{min} , the minor axis of the hot spot. On the best-resolved maps of such sources it is evident that the hot spots are disk-like, i.e. that the length of the downstream emission region is less than the diameter of the hot spot. The emission would fade rapidly if B decreased due to expansion, so we expect B not to decrease substantially where emission is observed. We assume for simplicity that B is constant in this downstream region.

The synchrotron loss equation for an isotropic distribution may be written as

$$dp/dt = -p^2 \beta, \quad (6)$$

where

$$\beta = \frac{2\sigma_T}{3m^2 c^2} \left(\frac{B^2}{\mu_0} \right), \quad (7)$$

and $\sigma_T = 6.65 \times 10^{-29} \text{ m}^2$ is the Thomson cross section. The solution of equation (6) for constant B is

$$p(t) = \frac{p_i}{1 + \beta p_i t}, \quad (8)$$

with $p(t) = p_i$ at $t = 0$. Hence, synchrotron losses are unimportant for $p(t) \sim p_i$, below a break point at $p_b \sim (\beta t)^{-1}$. We use the equipartition value B_{eq} for the magnetic field to calculate the synchrotron losses. Interpreting t in terms of the time taken to travel a distance $x = u_+ t$, we write (8) in the form

$$p(x) = \frac{p_i}{1 + \beta p_i x / u_+}. \quad (9)$$

3.3.2 Emitted synchrotron flux density

To calculate the emitted flux density, we approximate the synchrotron emissivity of a single electron by

$$j_\nu(p) = \frac{a_0 p B}{2a_1} \delta(p/mc - \sqrt{\nu/a_1 B}), \quad (10)$$

where $a_0 = 1.6 \times 10^{-14} \text{ W T}^{-2}$ and $a_1 = 1.3 \times 10^{10} \text{ Hz T}^{-1}$. The flux density emitted from the downstream electrons is then

$$F_{\text{ds}}(\nu) = \frac{l^2}{4\pi D_s^2} \int_0^\infty 4\pi p^2 dp \times \int_0^{l/2} dx j_\nu(p) f(p, x), \quad (11)$$

where D_s is the distance to the source. The electrons that are undergoing acceleration at the shock front also contribute to the radio emission, emitting a flux density

$$F_{\text{sh}}(\nu) = 4\pi \frac{(r+1)}{r} \frac{\kappa}{u_+} \left(\frac{l}{D_s} \right)^2 \times \int_{p_i}^\infty dp p^2 f'(p) j_\nu(p) \quad (12)$$

(Ball & Kirk 1992). Following Kirk (1994), we take $\kappa \sim 10^4 \kappa_{\text{Bohm}}$, where $\kappa_{\text{Bohm}} \sim cr_g/3$ and $r_g = p_\perp/(eB)$ is the gyroradius. The total emission from the hot spot is then

$$F_{\text{tot}}(\nu) = F_{\text{sh}}(\nu) + F_{\text{ds}}(\nu). \quad (13)$$

3.4 Expansion Losses

Since the secondary hot spot is observed to be larger than the primary, the plasma almost certainly expands between the shocks. We therefore include expansion losses in the region between the synchrotron loss region and the second shock. The transport equation which takes expansion losses into account is

$$\frac{\partial f}{\partial t} + \mathbf{u} \cdot \nabla f - \frac{1}{3} (\nabla \cdot \mathbf{u}) p \frac{\partial f}{\partial p} = 0. \quad (14)$$

From the observations (Valtoaja 1984) we assume a constant opening angle in the expansion region. Assuming cylindrical geometry, changing to the comoving frame and writing $R = r - v_r t$, the transport equation reduces to

$$\frac{\partial f}{\partial t} + \frac{v_r}{3(R + v_r t)} p \frac{\partial f}{\partial p} = 0. \quad (15)$$

The solution of (15) is

$$p(\tau) = p_i(\tau/\tau_i)^{-1/3}, \quad (16)$$

where $\tau = (R + v_r t)/v_r$ and $\tau_i = R/v_r$. Taking $R = l_1$, the size of the primary hot spot, and allowing the flow to expand to a diameter l_2 , a electron with an initial momentum p_i has a final momentum p_f given by

$$p_f = p_i(l_2/l_1)^{-1/3}. \quad (17)$$

3.5 Reacceleration

The distribution of electrons at the first shock, modified by synchrotron and expansion losses, is reaccelerated at the second shock, which terminates the flow. The total emission from the secondary hot spot is calculated as for the primary. The compression ratio of the second shock is a model parameter.

4 Results and Discussion

4.1 Results

The data that we attempt to model are given in Tables 1 and 2. Table 1 contains the observed

parameters, and Table 2 the parameters derived from those observed. In particular, we seek to model the spectral differences, i.e. the change in the radio spectral index, between the primary and the secondary hot spots in 3C 268.4, 3C 196 and 3C 20. The model used involves four free parameters, the spectral index of the electron distribution of the jet b_j , the compression ratios of the shocks in the primary and secondary hot spots r_1 and r_2 respectively, and the speed of the jet u_j . We assume $b_j = 4.2$, and vary r_1 to get the observed spectral indices of the first hot spot. The steepness of the resulting spectrum is determined by the smallest of b_j and $b_s = 3r_1/(r_1 - 1)$, where b_s is the spectral index of the accelerated electron distribution that would result from a δ -function injection. The jet speed u_j determines the length of time the electrons spend in the constant magnetic field region; it therefore determines the break frequency ν_b , which is related to the break momentum p_b by $\nu_b = (p_b/mc)^2 a_1 B$.

Figure 1 shows the evolution of the electron spectrum as it is accelerated by the shocks and undergoes losses. The injection spectrum (a) obeys a power law $f(p) \propto p^{-b_j}$. The spectrum immediately after acceleration at the primary shock is shown at (b). Synchrotron losses cause a spectral break at p_b (c). Expansion losses then move the spectrum down uniformly in p (d). The electrons are then reaccelerated by a weaker secondary shock to produce the spectrum shown at (e), and synchrotron losses occur again to produce the spectrum shown at (f).

The results of fitting the model to the sources 3C 268.4 and 3C 20 are shown in Figure 2 and summarised in Table 3. The results for 3C 196 are not shown in Figure 2 because of the failure of

Table 1. Measured values of radio fluxes at 408, 1666, 5000 and 15 000 MHz and sizes of the primary and secondary hot spots for 3C 268.4 (Lonsdale & Barthel 1986), 3C 196 (Lonsdale & Morison 1983) and 3C 20 (Hiltner et al 1994)

Component		S_{408} (mJy)	S_{1666} (mJy)	S_{5000} (mJy)	S_{15000} (mJy)	l_{\min} (kpc)	l_{\max} (kpc)
3C 196	A1	7100±400	3420±200	1600±200		1.6	5.2
	A2	8350±500		400±200		17	20
3C 268.4	A1		860±34		100±5	0.2	0.4
	A2		460±23		35±2	0.8	1.2
3C 20	A1			137±5	61±2	2	<3
	A2			137±5	51±2	20	20

Table 2. Calculated values of radio spectral indices and the equipartition magnetic field for the primary and secondary hot spots of 3C 268.4 (Lonsdale & Barthel 1986), 3C 196 (Lonsdale & Morison 1983) and 3C 20 (Hiltner et al. 1994)

Component		α_{408}^{1666}	α_{1666}^{5000}	α_{1666}^{15000}	α_{5000}^{15000}	α_{408}^{5000}	B_{eq} (nT)
3C 196	A1	-0.52	-0.69				56
	A2					-1.21	18
3C 268.4	A1			-0.98			~30
	A2			-1.17			~12
3C 20	A1				-0.73		~13
	A2				-0.90		~5

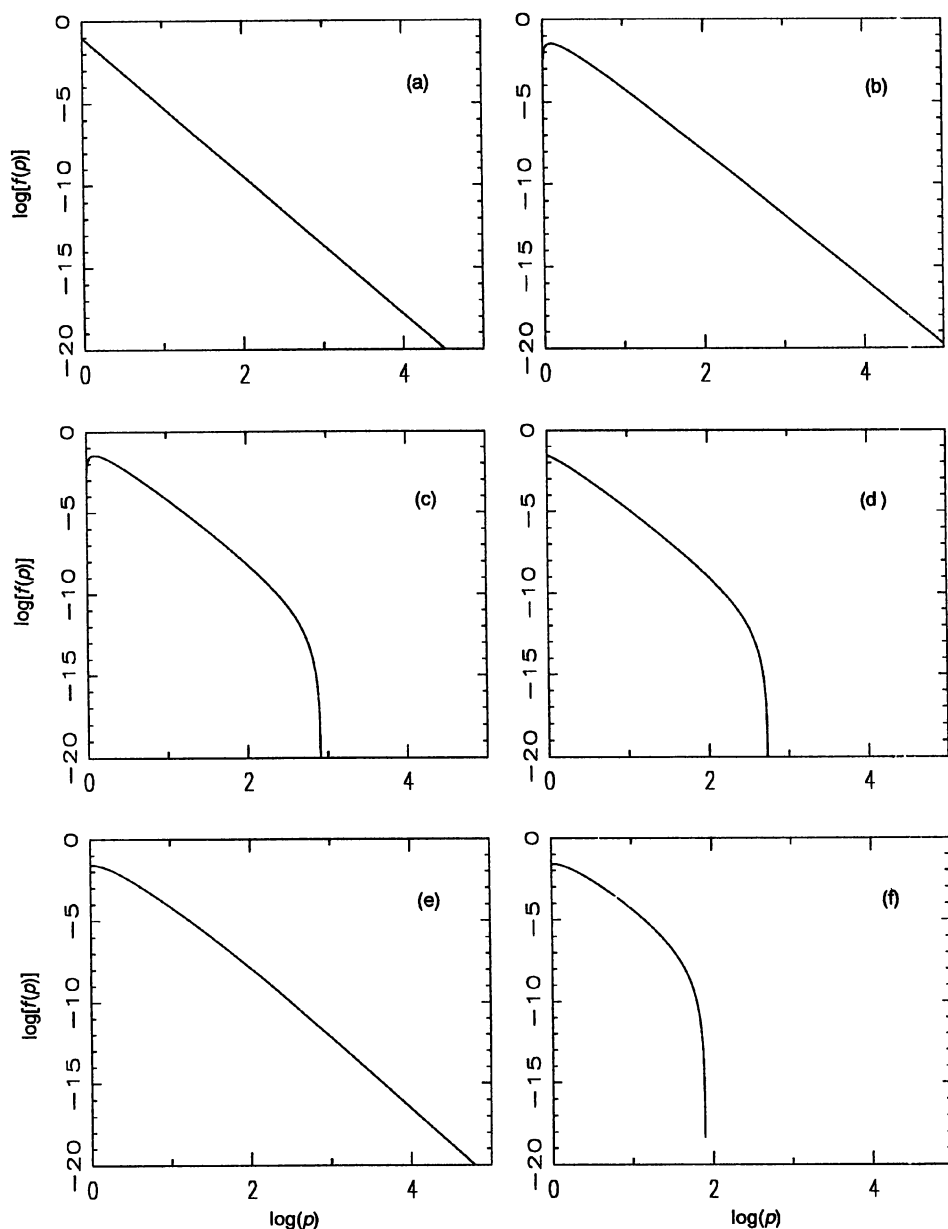


Figure 1—The stages of evolution of the distribution function $f(p)$ for various stages in the model: (a) the injection spectrum $f_{\text{inj}}(p) \propto p^{-4.2}$; (b) the spectrum immediately after acceleration at an $r_1 = 4$ shock; (c) after synchrotron losses in the primary hot spot; (d) after expansion losses between the hot spots; (e) after reacceleration at an $r_2 = 3.2$ shock; (f) after synchrotron losses in the secondary hot spot.

the model to reproduce the observations. Table 3 shows the values of our model parameters together with values of the spectral indices that the model produces, e.g. α_{408}^{1666} is the spectral index between 408 and 1666 MHz. The choice of u_j is only important where there is significant curvature in the observed spectra (such as in the primary hot spot of 3C 196), i.e. where the observations are near the

break frequency. In this case there are only two important variables, the smaller of b_j and b_s , and u_j . If the break frequency is either much higher or much lower than the frequencies of interest then the choice of u_j is not unique, and the results for the primary are determined only by the smaller of b_s and b_j . The spectrum of the secondary hot spot is then determined by r_2 .

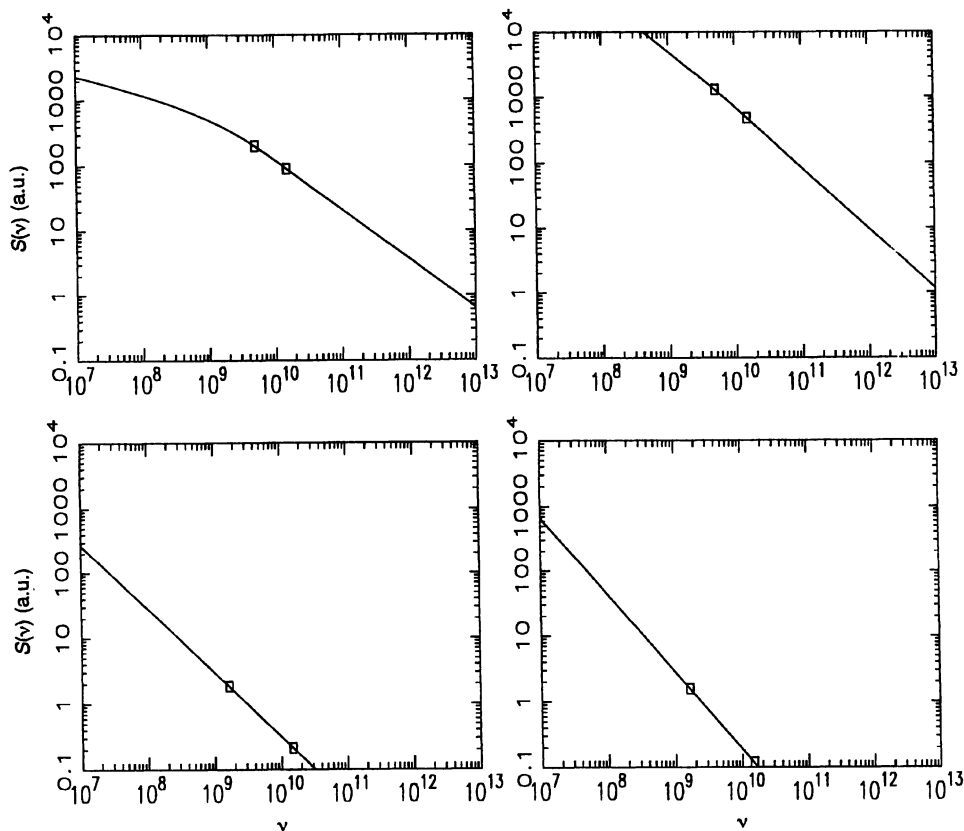


Figure 2—Spectra (flux density in arbitrary units versus frequency in Hz) for the primary (left) and secondary (right) hot spots of 3C 20 (top), and 3C 268.4 (bottom). The squares denote the observations scaled to the model flux levels.

Table 3. Model parameters and best-fit values of radio spectral index for the primary and secondary hot spots of 3C 268.4, 3C 196 and 3C 20

Component	u_j	r	v_j	α_{408}^{1666}	α_{1666}^{5000}	α_{1666}^{15000}	α_{5000}^{15000}	α_{408}^{5000}
3C 196	A1	c	7.0	4.0	-0.747	-0.748		
	A2		3.1					—
3C 268.4	A1	0.95 c	4.05	4.2		-0.979		
	A2		3.2			-1.182		
3C 20	A1	0.95 c	6.8	4.2			-0.729	
	A2		4.5				-0.900	

4.2 Discussion

The success of the model for each of the sources considered is discussed below.

4.2.1 3C 196

The model fails to reproduce the observations for 3C 196. The observed spectrum is too flat to be fitted by a simple DSA model. This suggests either that a more complicated model is required, or that parameters which were fixed in our model fits are incorrect, e.g. the magnetic field in the source may be less than the derived equipartition value, or the primary hot spot may be unresolved, in which case the value of l_{\min} used would be an overestimate.

Either of these two considerations would decrease synchrotron losses and flatten the model spectra.

4.2.2 3C 20 and 3C 268.4

The model successfully reproduces the observed spectra of 3C 20 and 3C 268.4. For both of these sources, a large primary shock compression ratio $r_1 > 4$ is required to reproduce the observations of the primary hot spot. This implies that there is a precursor region, upstream of the shock, in which relativistic electrons are important. The relevant adiabatic index for a relativistic fluid is $\gamma = 4/3$, allowing a maximum compression ratio $r = 7$. [For $r > 4$, one has $b < 4$ in equation (4), and there is

then infinite energy in the distribution if it extends to $p = \infty$; in practice the finite time of acceleration implies a finite upper limit to p , so that the energy in the distribution remains finite.] For 3C 20, $r_1 = 6.8$, which suggests that the precursor region may be dominated by the relativistic electrons. For 3C 268.4, we find $r_1 = 4.05$ and so the evidence for a relativistic electron precursor is not conclusive. The relatively high value of the compression ratio for the secondary hot spot of 3C 20, $r_2 = 4.5$, may suggest that our treatment of the secondary hot spot structure is oversimplified.

For both sources the implied jet velocity is large, $v = 0.95c$. This finding is in contrast to the results of M89, who considered only single hot spot sources, and found $\langle v \rangle = 0.3c$.

5 Conclusions

We present a model for the radio emission from extragalactic radio sources with two hot spots. Electrons are accelerated by diffusive shock acceleration, with synchrotron losses downstream of the shocks in regions of constant magnetic field, and with expansion losses between the shocks. The compact, flatter-spectrum primary is fed directly by the jet. The secondary is fed by the primary, forming a weaker shock at which the synchrotron-emitting electrons are reaccelerated. The resulting synchrotron spectrum of the secondary is steeper than that of the primary.

The model is consistent with the observations of 3C 20 and 3C 268.4, and thus may be appropriate for sources where the secondary appears to be a splatter spot (CGS; where the secondary is diffuse and is aligned roughly normal to the line of sight to the primary). For 3C 196, the model fails to reproduce the observations of the primary hot spot. The conclusion to be drawn from this is either that a more complicated model is required, or

that parameters which were fixed in the model are incorrect, e.g. that the magnetic field in the source is less than the derived equipartition value, or the primary hot spot is under-resolved.

Acknowledgments

The authors wish to thank the referee for useful comments. M.P. would like to thank R. Ekers and G. Bicknell for helpful comments on this work, and acknowledges support from an Australian Postgraduate Research Award.

- Achterberg, A., & Ball, L. 1994, *A&A*, 284, 687
 Anastasiadis, A., & Vlahos, L. 1993, *A&A*, 275, 432
 Ball, L., & Kirk, J. G. 1992, *ApJ Lett.*, 396, L39
 Bicknell, G. V. 1985, *PASA*, 6, 130
 Blandford, R. D., & Rees, M. J. 1974, *MNRAS*, 169, 395
 Bridle, H. A., & Perley, R. A. 1984, *ARA&A*, 22, 319
 Cox, C. I., Gull, S. F., & Scheuer, P. A. G. 1991, *MNRAS*, 252, 558 (CGS)
 Fanaroff, B. L., & Riley, J. M. 1974, *MNRAS*, 167, 31P
 Gopal-Krishna, & Wiita, P. J. 1990, *A&A*, 236, 305
 Kirk, J. G. 1994, in *Kinetic Plasma Physics*, ed. J. G. Kirk, D. B. Melrose & E. R. Priest (Berlin: Springer)
 Laing, R. A. 1981, *MNRAS*, 195, 261
 Laing, R. A. 1988, in *Hot Spots in Extragalactic Radio Sources*, ed. K. Meisenheimer & H.-J. Röser (Berlin: Springer), 27
 Laing, R. A., Riley, J. M., & Longair, M. S. 1983, *MNRAS*, 204, 151
 Lamont, P. J., & Hunt, B. L. 1980, *J. Fluid Mech.*, 100, 471
 Lonsdale, C. J., & Barthel, P. D. 1986, *AJ*, 92, 12 (LB)
 Lonsdale, C. J., & Morison, I. 1983, *MNRAS*, 203, 833
 Meisenheimer, K., et al. 1989, *A&A*, 219, 63
 Valtaoja, E. 1984, *A&A*, 140, 148
 Webb, G. M., Drury, L. O'C., & Biermann, P. 1984 *A&A*, 137, 185
 Williams, A. G. 1991, in *Beams and Jets in Astrophysics*, ed. P. A. Hughes (Cambridge Univ. Press), Ch. 7
 Williams, A. G., & Gull, S. F., 1984, *Nature*, 313, 3 (WG)
 Wilson, M. J. 1988, in *Hot Spots in Extragalactic Radio Sources*, ed. K. Meisenheimer & H.-J. Röser (Berlin: Springer), 315